MDPI

Development of Prediction Models for Pressure Loss and Classification Efficiency in Classifiers

Michael Betz *, Hermann Nirschl and Marco Gleiss

Institute for Mechanical Process Engineering and Mechanics (MVM), Karlsruhe Institute of Technology, 76131 Karlsruhe, Germany; hermann.nirschl@kit.edu (H.N.); marco.gleiss@kit.edu (M.G.)
* Correspondence: michael.betz@kit.edu

Abstract: This paper presents the development of prediction models for pressure loss and classification efficiency in classifiers. Classifiers belong to one of the most important classification devices in gas particle processing and a fast and accurate determination of pressure loss and cut size is of great interest. The first model developed in this work allows the calculation of pressure loss as a function of geometric and operational parameters. It is based on a number of measured values that are obtained from previous numerical simulations (CFD). The maximum deviation of the model less than 20% and the model operates in real time. However, the model requires calibration for each type of classifier. The second model for classification efficiency is based on a simplified two-dimensional approach in which the flow profile and particle trajectories are determined exclusively for the area between two classifier blades. The model is applicable for all geometrical and operational parameters and calculates the desired parameters within a few minutes, with a maximum error rate of 25%. In combination, the two models allow for the process optimization of classifiers in complete systems.

Keywords: air classifier; CFD; optimization; classification performance

1. Introduction

In solid processing technology, centrifugal classifiers play an important role in the classification of gas particle mixtures [1–3]. Centrifugal classifiers belong to the category of countercurrent classifiers that uses a forced vortex flow. A force equilibrium between the centrifugal and drag forces acts as the separation principle. Coarse particles are rejected at the classifier wheel due to the high centrifugal forces, while finer particles are transported inward by the air and then discharged due to the dominant drag force [4]. Due to the rotation of the rotor, centrifugal classifiers have a low sensitivity to changes in solid loads and the separation characteristics can be well controlled by the speed of the classifier [5]. This allows for a wide range of applications, which is why classifiers are used in the mineral, chemical and pharmaceutical industries [6–8].

A large number of studies have been carried out to establish a better understanding of flow processes in classifiers. These can be divided into optical methods, such as laser Doppler anemometry (LDA) measurements and particle image velocimetry (PIV), or computational fluid dynamics (CFD). For example, Toneva [9] experimentally investigated the flow and demonstrated that the flow separates in the region between two classifier wheel blades, creating vortices that constrict radial air transport into the interior of the classifier wheel. This results in a shift of the classification performance to coarse particles. Furthermore, both Stender and Spötter [10,11] were able to physically observe the separation process between two classifier wheel blades. Their investigations prove that particle–wall and particle–particle collisions intensively influence particle motion. Accordingly, as the speed of rotation increases, particle movement is focused on the trailing blade, resulting in an increased number of collisions in this zone. Thus, material deposited on the classifier wheel mainly accumulates outside the classifier wheel, while the fine particles inside are

rapidly transported toward the exit. A large number of other researchers have now confirmed these observations [12–14] and the consensus is that the decision as to whether a particle is deposited on the classifier wheel occurs primarily between two classifier blades. Furthermore, the pressure loss mainly results from high velocities inside the classifier wheel [15,16].

The costs and time required for experimental studies are very high, which is why numerical flow simulation is primarily used for optimization, depending on the geometric structure or operating conditions [17–19]. However, numerical studies also require a certain amount of time, which is why the time required for process optimization must be further reduced. Process optimization means the consideration of the classification process with regard to the entire system, since comminution steps or other processing steps are often integrated and the individual process steps influence each other. Therefore, the creation of mathematical models for the prediction of characteristic parameters, such as pressure loss and the separation behavior of classifiers as a function of geometric and operational parameters, is of great interest.

So far, modeling approaches are only available for the cut size. While Yu [20] follows a purely empirical approach, Spötter's model [11] is more oriented to physical relationships. Based on a trajectory model between two classifier blades, the trajectories of particles of different sizes are approximated and the cut size is calculated from a force equilibrium. Subsequently, the cut size function can be calculated with the help of the model by Molerus [21]. Particle–wall and particle–particle collisions are estimated with the help of scaling equations. These are material-specific and are obtained from experiments. Furthermore, an experimental or numerical determination of the flow profile is required, which increases the current time expenditure of the model.

This paper presents models for calculating the pressure loss and cut size in centrifugal classifiers. The pressure loss in classifiers is caused by the required energy input for the fluid to flow through the whole apparatus. Since there is no simple physical relationship for the pressure loss, a purely empirical approach was taken. The model was based on a large number of measured values for various operational and geometrical parameters, which were obtained from numerical simulations. For the cut size, Spötter's model was further developed. In order to obtain faster information for the flow profile between two classifier blades, a simplified two-dimensional simulation approach that was based on Spötter's model was implemented.

2. Materials and Methods

2.1. Model for Pressure Loss

Although the pressure loss in a centrifugal classifier mainly occurs in the inner area of the classifier, it seems impossible to derive a mathematical model that describes all of the different geometric properties of a classifier at all operating conditions that affect the pressure loss. This is one of the reasons why no approach for predicting the pressure loss exists yet. However, in developing a mathematical model, we can take advantage of the fact that manufacturers standardize their process when designing classifiers and always leave certain geometric properties the same when scaling up. This reduces the number of different parameters and allows for an empirical model to be developed for at least one type of classifier from one manufacturer. Geometric properties can also be integrated into this model, but the effort increases with each parameter that is investigated. In this paper, we present the development of a mathematical model for a single classifier with a tangential inlet that is frequently used in practice. In the investigation, the speed of the classifier, the volume flow rate and the feed size were varied under the operating conditions. The geometrically modified factors were the diameter of the classifier wheel and the height to diameter ratio of the classifier wheel. It would be interesting to include other factors, such as the diameter of the duct removing the air from inside the classifier and the angle of the classifier wheel blades, as these also have a great influence on the pressure loss. The more parameters that are integrated into a model, the more the scope of the mathematical

model grows. In order to compare different classifier wheel sizes, it is advisable to express the operating conditions independently of size. Therefore, the speed of the classifier, the volume flow and the feed size were converted into the acceleration of the classifier wheel, the average radial velocity and the solid loading.

The classifier used to describe the mathematical model and its geometric dimensions are schematically sketched in Figure 1. A detailed description of the different parameters can be found in [22]. In this type, the air enters from the outside via a tangential air inlet and is aligned using static guide blades. It then flows inward through the classifier wheel blades and is discharged downward inside the classifier wheel. The material is fed above the classifier, between the static guide blades and the classifier wheel. A baffle disk is used to distribute the material evenly. The material is picked up by the air and transported toward the classifier. In the scale-up, geometrical factors, such as the distance between two static guide blades and two classifier wheel classifier blades, remain identical. Other parameters, such as the duct diameter, are scaled equally to the change in size of the classifier wheel diameter.

1 Air Inlet
2 Feed material
3 Coarse material
4 Air + fine material
5 Rotor cage
6 Static guide blades
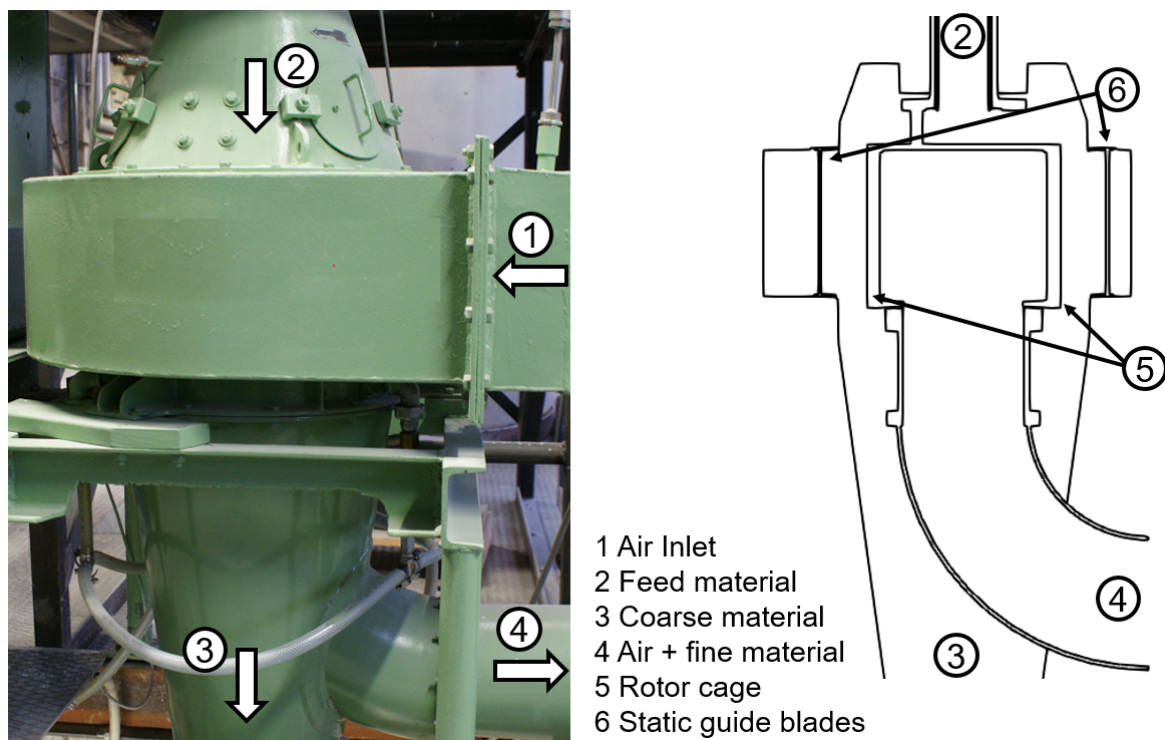
Figure 1. A schematic view of the investigated classifier [22].

The mathematical model was based on an algorithm that estimates the influence of various geometric and operational parameters using derived functions. To determine the functions, a number of measured values was required as a function of the parameters under investigation. These were determined with the help of the numerical flow simulation since an experimental determination was impossible for time and cost reasons. The numerical simulation took place in the software environment OpenFOAM-6 with the solver SimpleFoam. The influence of the dispersed phase was neglected in the simulations. An estimation of the influence of different solid loading on the pressure loss follows later. In the simulations, the flow was considered as an incompressible, isothermal Newtonian fluid. Therefore, the velocity and pressure profile could be determined by solving the Navier–Stokes equations. These were obtained from the continuity and momentum equations to obtain:

$$\rho \nabla \vec{u} = 0 \tag{1}$$

$$\frac{\partial \rho \vec{u}}{\partial t} + \rho(\nabla \cdot \vec{u})\vec{u} = -\nabla p + \eta \Delta \vec{u} + \vec{f} \tag{2}$$

where ρ is the density, $\vec{u}$ is the velocity vector, η is the viscosity and $\vec{f}$ is the external volume forces. The turbulence was modeled using the k–ω SST model, which has been proven in previous simulations [22]. The rotation of the classifier was performed using the Multiple Reference Frame (MRF) approach. The MRF approach calculates the flow in a rotating and stationary reference system. The rotating components were thus frozen in a fixed position and the model solved the Navier–Stokes equations for the flow with additional centrifugal and Coriolis forces. Accordingly, the MRF model does not consider any transient effects, which was fine since only a steady-state solution was required to determine the pressure loss. These are common methods for the determination of the pressure loss in classifiers and have already been widely tested [12,14–16].

The boundary conditions are listed in Table 1. At the walls, no-slip was defined for the velocity, while the volume flow for the experiments was specified at the inlet. At the outlet, a relative pressure of 0 Pa was set. The outlet had to be defined in the simulations at a certain distance from the inside of the classifier wheel so that the strongly occurring vortices were not influenced by the boundary conditions. The material inlet and coarse material outlet were also defined as a wall since, in the experiments, the material was supplied and discharged in an airtight manner.

Table 1. The boundary conditions.

	Inlet	Outlet	Wall
Velocity	Fixed value	Zero gradient	No-slip
Pressure	Zero gradient	Total pressure of 0 Pa	Zero gradient

The calculation of the Navier–Stokes equations was discrete, which is why it was necessary to transform the geometry of the classifier into a grid. For a faster and better result, smaller edges and corners were simplified. In this work, the meshing of all geometries was performed with the meshing tool SnappyHexMesh, which is freely available in OpenFOAM and generates an unstructured hexahedral mesh with prism layers. The thickness of the prism layers could also be used to control the y+ value required for the turbulence model. This had to be less than five. For the different classifiers, three different grids were created. Thus, a grid study could be performed and the effect of a grid on the result could be excluded. As an example, Table 2 shows the calculated pressure loss for a classifier wheel with an outer diameter of 0.32 m compared to the experimental pressure loss of the three grids. The medium grid was chosen because it represents a good compromise between accuracy and computational effort. A representation of the grid is shown in Figure 2.

Table 2. A comparison between the simulated and experimental pressure loss of the three grids.

Grid	Number of Elements	Pressure Loss in Simulation (Pa)	Standard Deviation to Experiment (%)
Coarse grid	7.4 m	2213	20.9
Medium grid	11.5 m	2521	9.8
Fine grid	15.3 m	2576	7.9
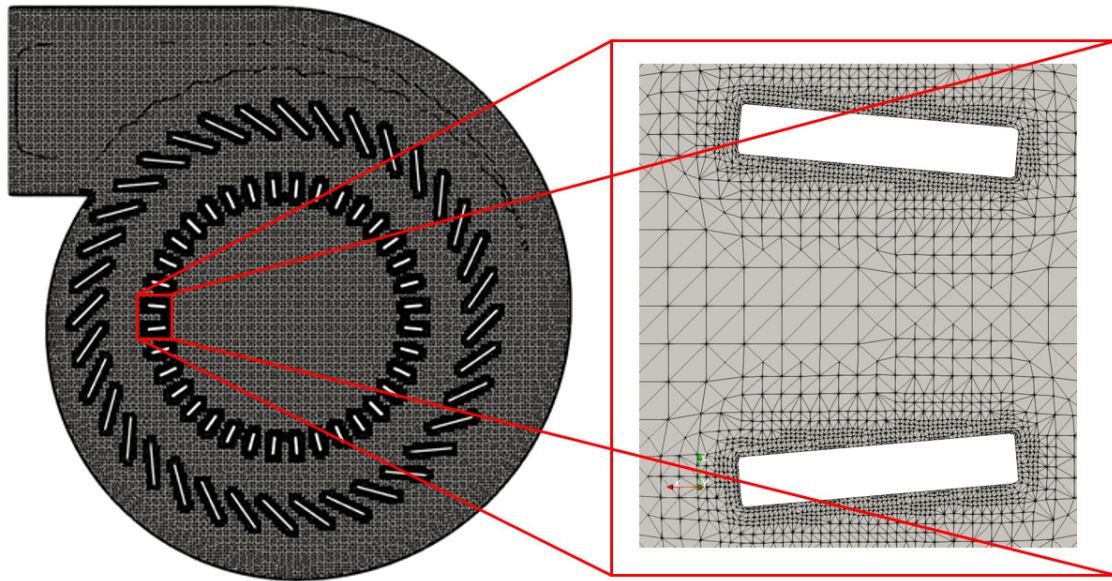
Figure 2. A horizontal slice of the mesh of the classifier.

To validate the numerical calculations, the results of the pressure loss were compared to the experimentally measured results under different operating conditions. The left-hand side of Figure 3 shows the comparison of different accelerations and radial velocities for a classifier with a diameter of 0.32 m. The figure proves that the calculated values had a pressure loss that was about 10–15% lower. This was probably due to the turbulence model. Other studies have already shown that a two-equation model, such as the k–ω SST model, can only represent the highly turbulent flow in a classifier to a limited extent [22]. In addition, the simplifications of the geometry also naturally led to a reduced pressure loss. However, the deviations were sufficiently small that a correction function could be used to determine the values.

(**a**)

(**b**)
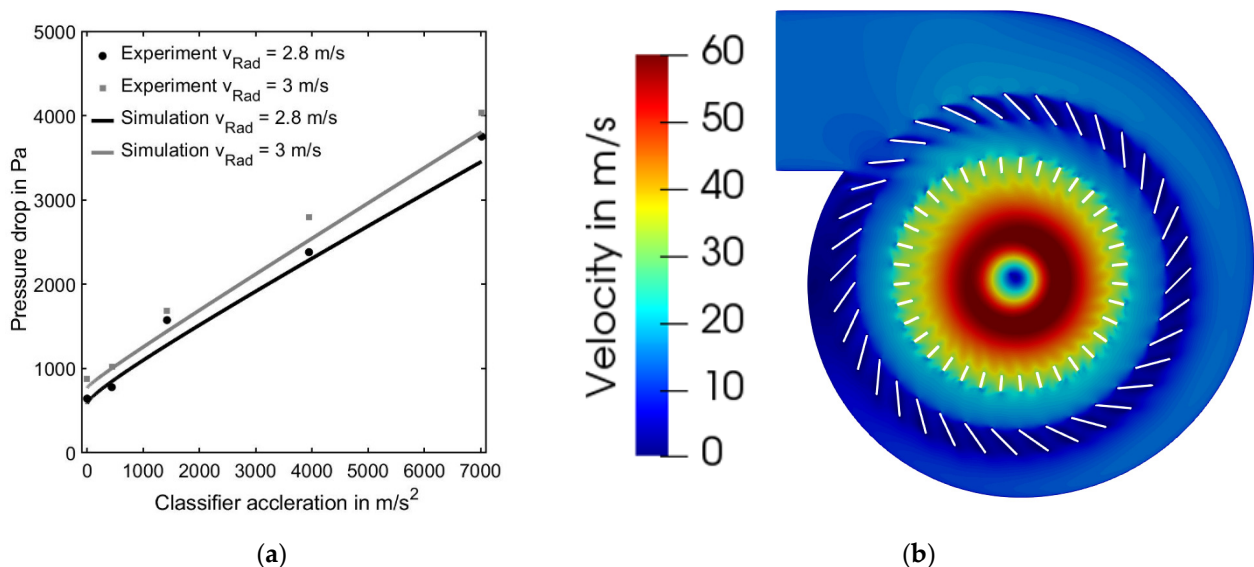
Figure 3. (**a**) A comparison of the calculated and measured pressure loss for different operating conditions; (**b**) the velocity profile in the classifier.

In addition, the flow profile was compared to illustrations from the literature. The right-hand side of Figure 3 shows the flow profile of the classifier as a horizontal section. This shows that the highest velocities were inside the classifier. Toneva [9] has already

described the flow profile in detail and divided it into three sections. The profile here also shows these sections, which can be considered as proof of the accuracy of the numerical simulations. More detailed information on the flow profile and pressure loss of this classifier can be found in a previous study [22].

The numerical solver could then be used to determine the pressure loss for a wide range of different operating conditions and geometries. The functions required for the mathematical model were then derived from this. Figure 4 shows examples for the different accelerations, radial velocities, classifier wheel diameters and height to diameter ratios of the classifier wheel. The individual curves also reveal the influence of each parameter. The graphs show that, as expected, the pressure loss in the classifier increased with increasing acceleration or radial velocity. Increasing the classifier wheel diameter also increased the pressure loss. The simulations further demonstrated that the pressure loss also varied strongly as a function of the height to diameter ratio.

(a)

(b)

(c)
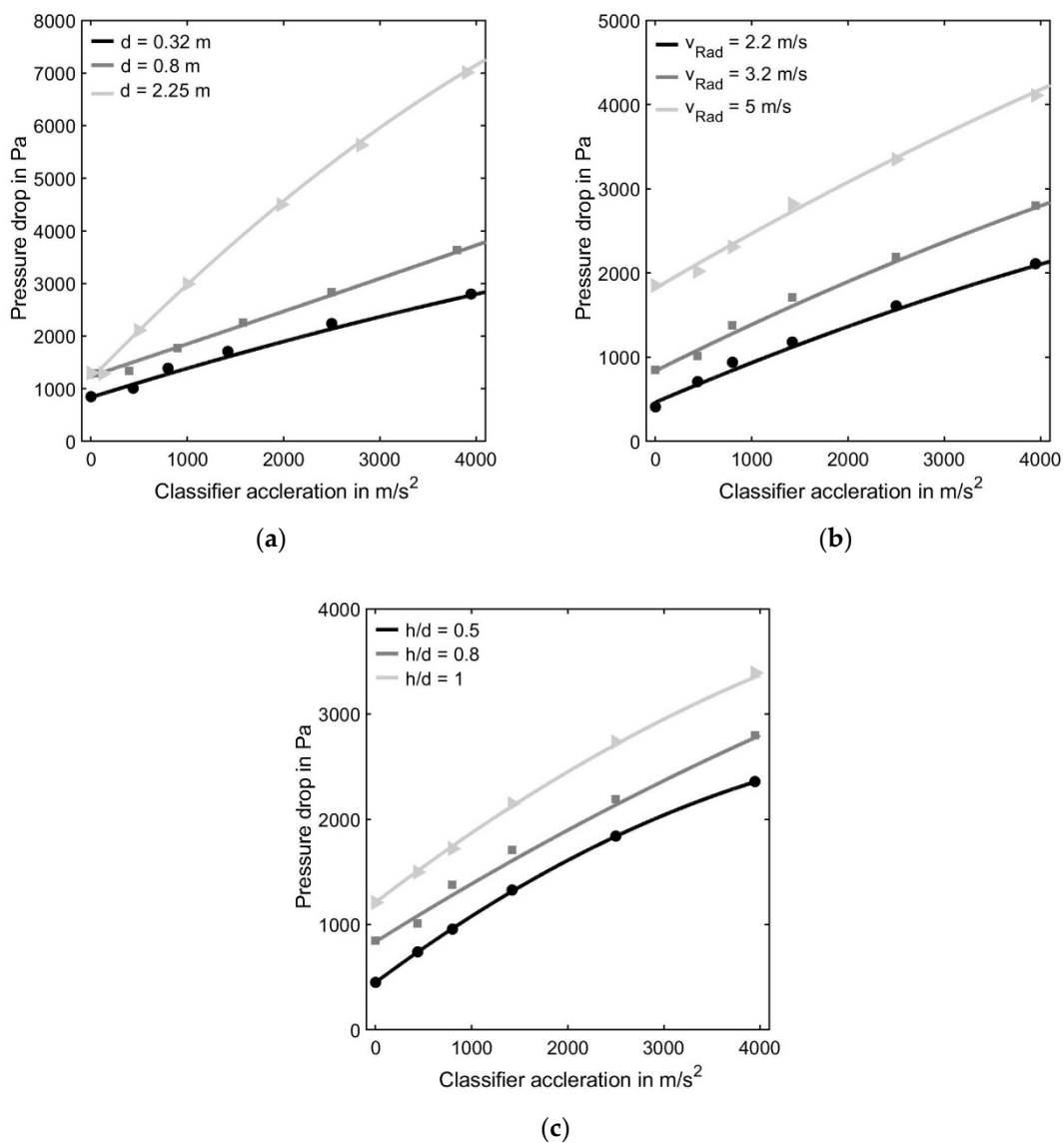
Figure 4. The corrected pressure loss from the numerical calculation as a function of (**a**) acceleration and classifier diameter, (**b**) acceleration and radial velocity and (**c**) acceleration and height to diameter ratio.

In previous studies, the influence of the dispersed phase has been neglected. A comparison of the pressure loss of an unloaded and loaded flow showed that the additional

pressure loss caused by the material correlated strongly with the solid loading in the fine particles. This was due to the fact that the material entering the inside of the classifier wheel had to be accelerated by the flow. Figure 5 plots the pressure difference between unloaded and loaded flow versus solid loading. The function also describes the influence of the solid loading on the pressure loss. This was integrated into the mathematical model.
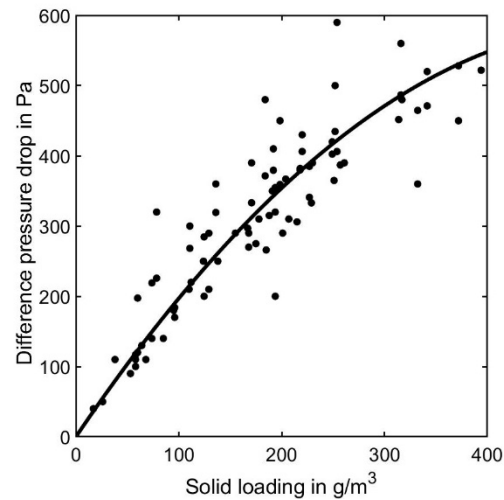
Figure 5. The pressure loss difference between unloaded and loaded flow as a function of solid loading under different operating conditions.

2.2. Model for Cut Size

Previous investigations on the separation behavior of classifiers have shown that the separation process takes place between two classifier blades. With the assumption that the flow profile of a deflector classifier is rotationally symmetric and that there is a uniform distribution over the axial height, Spötter [11] has already proved that the classification efficiency can be determined exclusively from the trajectories of the particles between two classifier blades. Stochastic effects, such as particle–particle collisions between the classifier blades, are therefore superimposed onto a possible non-uniform distribution of the flow. The time-consuming modeling of the classification efficiency mainly results from the determination of the velocity and pressure profile. However, when the influence of axial effects is neglected, the flow profile can be determined in a short time by cleverly setting the boundary conditions with the help of a simplified two-dimensional numerical approach. Subsequently, the classification efficiency can be determined directly on the basis of the motion paths of individual particles of different sizes. Figure 6 shows the area in a classifier that is required for the determination of the flow profile.
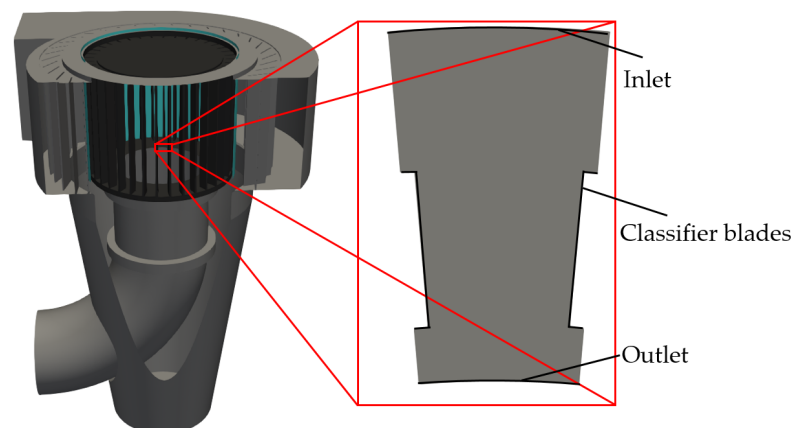
Figure 6. The simulated area for two-dimensional simulation.

The aim of this study was to exclude any influences on the flow profile due to the boundary conditions. Therefore, firstly, the inlet was limited by the inner edge of the static guide vanes. It was assumed that the volume flow was uniformly distributed over the inlet surface, which is why the radial velocity was derived from the average radial velocity for a three-dimensional consideration. The tangential velocity at the inlet results from the angle of the static guide blades. Secondly, the outlet was at the radial level of the outer edge of the duct. Effects due to geometrical installations inside the classifier could not be reproduced in a two-dimensional determination of the flow field. However, their influence was small since the flow field between the classifier blades was mainly characterized by the rotating blades. Thirdly, the estimation of material influences on the flow profile was difficult with a two-dimensional approach since material deposited on the classifier accumulated in front of the classifier wheel and sedimented in the direction of the coarse material discharge. A two-dimensional view did not provide any information on the solid loading in front of the classifier wheel, which is why the material deposited on the classifier wheel was removed from the simulation and declared as coarse material in the simulations carried out here.

While in Spötter's model, the cut size is determined from a force equilibrium between the acting centrifugal and drag forces, the classification efficiency could be determined here directly by tracking the particles of different sizes. Here, a discrete phase model (DPM) was used to track the particle motion. The equation of motion for an individual particle could be written as follows:

$$m_P \frac{du_P}{dt} = D_P(u_F - u_P) \tag{3}$$

where m_P is the mass of the particle, u_P is the velocity of the particle and u_F is the velocity of the fluid. Other forces, such as virtual mass force or lift forces, were negligible due to the low density ratio of fluid to solid. The term on the right-hand side is the drag force. OpenFOAM offers a number of different models to calculate drag force. In this work, a model was used that estimated the non-sphericity of the particles. In the simulations, the value for non-sphericity was 0.8 since these settings produced the best agreement with the experiment. For an estimation of particle–particle and particle–wall collisions, it is recommended to introduce scaling laws for an effective viscosity and the coefficient of restitution depending on material and particle velocity, which is similar to the model of Spötter. A complete consideration of particle–particle collisions could be integrated into the model, but the time required to model the collisions was enormous.

Figure 7 shows the particle distribution and particle trajectories in a 2D simulation. Due to the MRF approach and the focus on two classifier blades, the classifier blades remained stationary in the simulation and the particles moved relative to the classifier. The classifier rotated clockwise. Outside of the classifier wheel, the particles had a lower tangential velocity than the classifier, which is why they moved against the direction of rotation of the classifier and collided with the trailing blade. Fine particles continued to move inward before colliding and reached the inside due to the drag force, while the coarse particles bounced outward.

The reduction in the simulation area to a simplified two-dimensional view reduced the time required for the two-phase simulations enormously. In addition, the grid generation, which is very time-consuming in numerical simulation, could be automated. With the help of the program Matlab and the OpenFOAM tool blockMesh, an automated grid generation routine was created, which generated the grid in a few seconds depending on the size and shape of the classifier blades. Figure 8 shows the flowchart of the model. Subsequently, the flow profile and the particle paths were calculated, from which the cut size was determined.
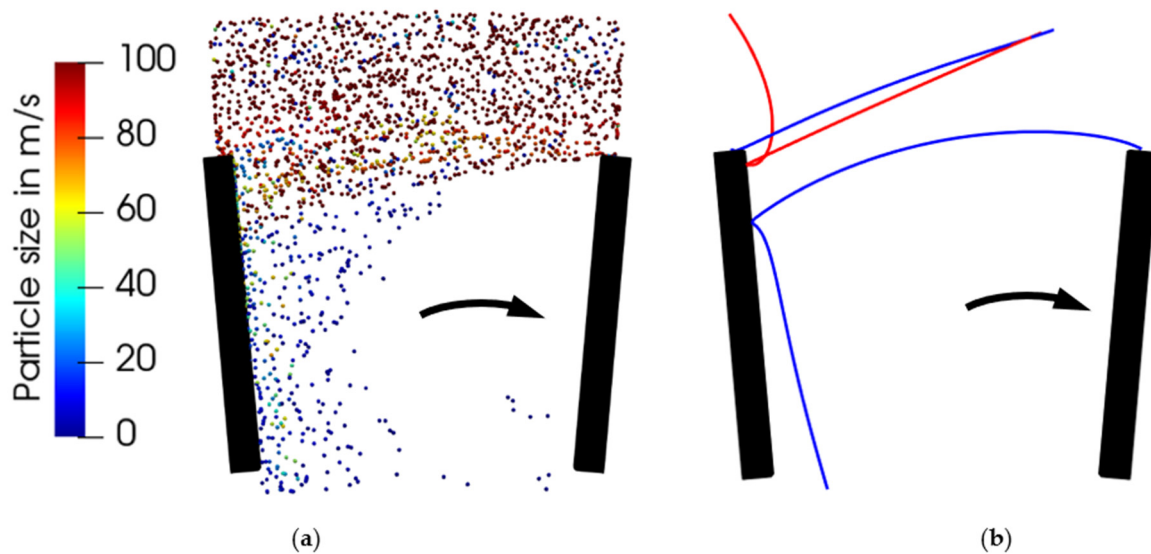
Figure 7. (**a**) Particle size distribution in front of and between classifier blades; (**b**) particle trajectories for a particle with a size of 10 μm (blue) and 60 μm (red).
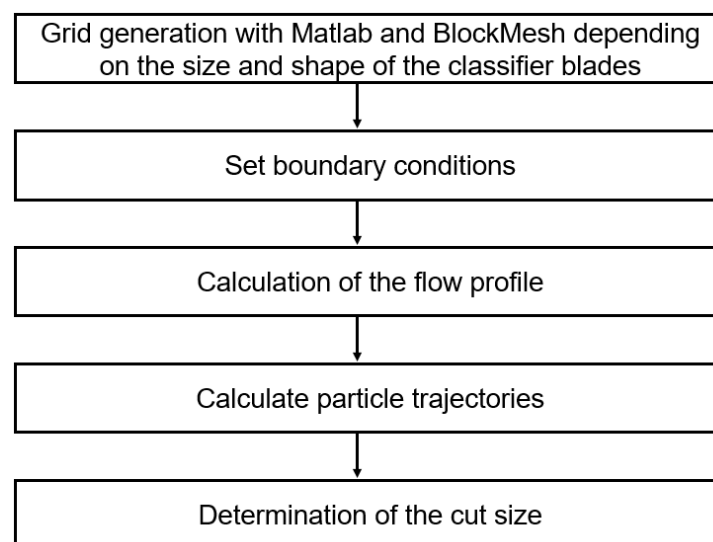
Figure 8. A flowchart for the cut size model.

3. Results

3.1. Results of the Pressure Loss Model

The accuracy of the created mathematical model for the pressure loss is provided in Figure 9, where the calculated values for the pressure loss are compared to experimentally measured data. The measured data were from real existing plants. In order to verify the model for a wide range, the comparison data for the diameter of the classifier varied in the range of 0.32 to 2 m, the data for the accelerations varied from 0 to 4000 m/s^2, the data for the radial velocities varied from 2.5 and 4.8 m/s and the data for the solid loadings varied from 0 to 450 g/m^3. In addition, the material used also varied. Unfortunately, no data were available for classifier wheels with different height to diameter ratios, so this parameter could not be verified. The comparison shows that the model developed in this work provided a very good agreement for most of the operating points. The deviation was only above 10% for one operating point (19.7%). It must be emphasized, however, that a comparison of the mathematical model could only be carried out on four existing classifiers. Nevertheless, the results obtained so far are extremely satisfactory since, after a single

adaptation of the mathematical model for one type of classifier, it was possible to directly determine the pressure loss as a function of the geometrical and operating parameters. This enabled the fast and targeted design of the classifier wheel for the pressure loss in the overall process.
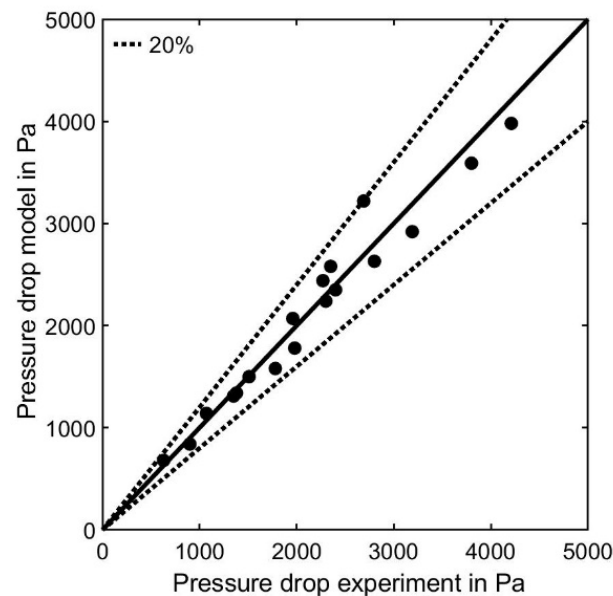
Figure 9. The comparison between the pressure loss in the mathematical model and the experiment with different systems.

The previous effort to create the functions required for the mathematical model was highly dependent on the number of parameters being studied. As a rule, in addition to the three most important operating parameters of radial velocity, acceleration and solid loading, the classifier wheel diameter is sufficient. The inclusion of other geometrical factors is of course of interest, but practice has shown that manufacturers usually follow a design thread depending on the classifier wheel diameter. For an optimization of the geometric structure, the numerical flow simulation showed advantages anyway. Nevertheless, the mathematical model showed that it could also provide insights into the understanding of flow processes. This is another reason why the formulation of a correlation between the solid loading and pressure loss was possible.

3.2. Results of the Cut Size Model

The inaccurate determination of the cut size by the model was due to two possible causes. First, the flow profile might have been incorrect due to the simplified two-dimensional approach. This error could only be corrected to a limited extent. On the other hand, the modeling of the particle trajectories could also have been inaccurate. In this case, the scaling laws for the effective viscosity and the coefficient of restitution, which estimated the influence of particle–particle and particle–wall collisions, were in the focus. Table 3 compares the cut size from the experiment, the model and a two-dimensional numerical simulation with the resolution of particle–particle collisions performed by the CFD-DEM approach under different operating conditions. The investigations referred to a classifier wheel with a diameter of 0.32 m. A simulation of particle–particle collisions with a CFD-DEM approach was very time-consuming compared to the model.

Table 3. The comparison of the cut size of the experiment, the mathematical model and the simulation of particle–particle interaction under different operating conditions.

Acceleration (m/s^2)	Radial Velocity (m/s)	Solid Loading (g/m^3)	Cut Size Experiment (µm)	Cut Size Model (µm)	Cut Size with CFD-DEM (µm)
439	2.2	250	60	52	54
1421	2.6	250	35	29	31
3947	2.6	250	21	17.5	18.5
1421	3.2	200	44	38	41

To date, no detailed scaling laws for the effective viscosity and the coefficient of restitution are available for the model as these generally require detailed experimental determination. The values presented in Table 3 are for a fixed restitution coefficient of 0.25. The viscosity was calculated from the existing solid loading per grid cell element in the simulation. Table 3 shows that the model provided about a 10–20% lower cut size than the experiment. The cut size calculated from elaborate CFD-DEM simulations showed minimally smaller deviations. It can be concluded from this that the deviation of the model from the experiments could be further reduced by adjusting the scaling laws. However, the calculated cut sizes were always lower than those determined experimentally. This leads to the assumption that the flow profile determined by the two-dimensional approach in conjunction with a focus on the area between two classifier blades is not sufficient to obtain more accurate results. Apparently, axial differences or the sometimes non-uniform rotational symmetry in the air distribution caused the separation conditions to be worse in individual areas of the classifier. This is also confirmed by Figure 10, where the comparison between the calculated and experimentally determined separation curves for different operating points is shown. Nevertheless, the model was able to reproduce the cut size for all classifier geometries and operating conditions that were investigated, with a maximum deviation of 25%.
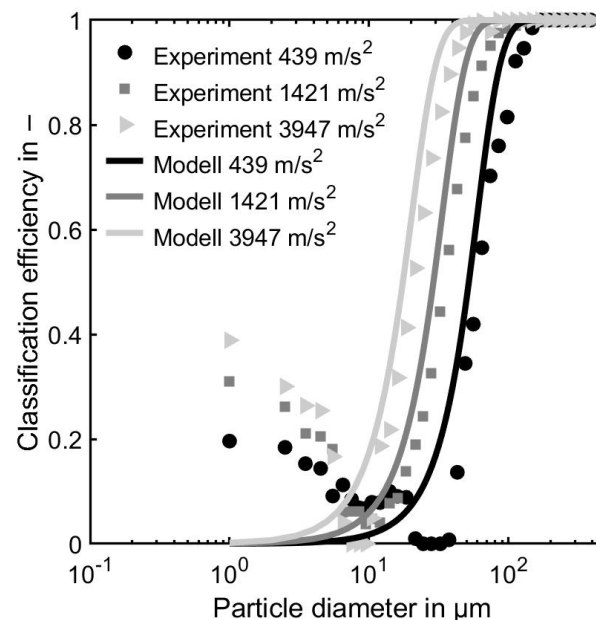
Figure 10. The comparison between the cut size curve of the model and the experiment for different classifier accelerations.

This is surprisingly good considering the complexity of the separation process, as the described model calculated information on the separation properties of the classifier for different geometrical and operational factors within a few minutes. Furthermore, it is noticeable that the model has not yet been designed to reproduce the fish-hook effect that occurs in experiments. The fish-hook effect is caused by the agglomeration of very small particles due to interparticle forces, which have not yet been taken into account in this model.

4. Conclusions

This paper dealt with the development of a prediction model for the pressure loss and classification efficiency in a centrifugal classifier. The aim of the two models was to provide information on the two most important parameters of the classifier as a function of geometrical and operational parameters in the shortest possible time and with sufficient accuracy. The model for the pressure loss followed an empirical approach in which the influence of the various geometric and operational parameters was integrated into the model via functions. The functions were derived from a set of measured values obtained by numerical simulations. A comparison between the experimentally determined and calculated values showed that the model is capable of calculating the pressure loss with an accuracy of < 20% within a few seconds. However, the model must be calibrated for each classifier type as the effort increases with increasing geometric parameters.

The model for calculating the cut size was a simplified two-dimensional approach for the area between two classifier blades. Since the separation of the coarse particles from the air stream occurs in this zone, the numerical calculation of the flow profile and particle trajectories in this zone was sufficient. This could significantly reduce the time required, allowing the calculation of the cut size to be completed in just a few minutes. The comparison between the classification efficiency curves of the experiment and the model showed that, despite the simplified approach, only maximum deviations of less than 25% occur. This is impressive since the separation process is very complex and the model is suitable for all geometric and operational parameters. However, it is noticeable that the model was not able to reproduce the fish-hook effect that occurs in experiments. This is due to the fact that interparticle forces were neglected. Furthermore, more comparisons of different classifier types and sizes need to be performed to further verify the model. Additionally, thermal aspects have also been completely neglected so far. Nevertheless, this work provides an important support for the process optimization of classifiers since the reduction in the computing time is required. In addition, it is also possible to improve the accuracy of the model by integrating scaling laws.

Abbreviations

The following abbreviations are used in this manuscript:

CFD   Computational Fluid Dynamics
DEM   Discrete Element Method
LDA   Laser Doppler Anemometry
MRF   Multiple Reference Frame
PIV   Particle Image Velocimetry
RANS   Reynolds-Averaged Navier–Stokes

References

1. Shapiro, M.; Galperin, V. Air classification of solid particles: A review. *Chem. Eng. Processing* **2005**, *44*, 279–285. [CrossRef]
2. Batalović, V. Centrifugal separator, the new technical solution, application in mineral processing. *Int. J. Miner. Processing* **2011**, *100*, 86–95. [CrossRef]
3. Johansen, S.T.; de Silva, S.R. Some considerations regarding optimum flow fields for centrifugal air classification. *Int. J. Miner. Processing* **1996**, *44–45*, 703–721. [CrossRef]
4. Bauder, A.; Müller, F.; Polke, R. Investigations concerning the separation mechanism in deflector wheel classifiers. *Int. J. Miner. Processing* **2004**, *74*, 147–154. [CrossRef]
5. Galk, J.; Peukert, W.; Krahnen, J. Industrial classification in a new impeller wheel classifier. *Powder Technol.* **1999**, *105*, 186–189. [CrossRef]
6. Wang, X.; Ge, X.; Zhao, X.; Wang, Z. A model for performance of the centrifugal countercurrent air classifier. *Powder Technol.* **1998**, *98*, 171–176. [CrossRef]
7. Kaczynski, J.; Kraft, M. Numerical Investigation of a particle separation in a centrifugal air separator. *Trans. Inst. Fluid-Flow Mach.* **2017**, *135*, 57–71.
8. Huang, Q.; Liu, J.; Yu, Y. Turbo air classifier guide vane improvement and inner flow field numerical simulation. *Powder Technol.* **2012**, *226*, 10–15. [CrossRef]
9. Toneva, P.; Epple, P.; Breuer, M.; Peukert, W.; Wirth, K.E. Grinding in an air classifier mill—Part I: Characterisation of the one-phase flow. *Powder Technol.* **2011**, *211*, 19–27. [CrossRef]
10. Stender, M.; Legenhausen, K.; Weber, A.P. Visualisierung der Partikelbewegung in einem Abweiseradsichter. *Chem. Ing. Tech.* **2015**, *87*, 1392–1401. [CrossRef]
11. Spötter, C.; Legenhausen, K.; Weber, A.P. Separation Characteristics of a Deflector Wheel Classifier in Stationary Conditions and at High Loadings: New Insights by Flow Visualization. *Kona Powder Part. J.* **2018**, *35*, 172–185. [CrossRef]
12. Barimani, M.; Green, S.; Rogak, S. Particulate concentration distribution in centrifugal air classifiers. *Miner. Eng.* **2018**, *126*, 44–51. [CrossRef]
13. Adamčík, M. Limit Modes of particulate Materials Classifiers. Ph.D. Thesis, Brno University of Technology, Brno, Czech Republic, 2017.
14. Ren, W.; Liu, J.; Yu, Y. Design of a rotor cage with non-radial arc blades for turbo air classifiers. *Powder Technol.* **2016**, *292*, 46–53. [CrossRef]
15. Guizani, R.; Mhiri, H.; Bournot, P. Effects of the geometry of fine powder outlet on pressure drop and separation performances for dynamic separators. *Powder Technol.* **2017**, *314*, 599–607. [CrossRef]
16. Betz, M.; Gleiss, M.; Nirschl, H. Effects of Flow Baffles on Flow Profile, Pressure Drop and Classification Performance in Classifiers. *Processes* **2021**, *9*, 1213. [CrossRef]
17. Liu, R.; Liu, J.; Yuan, Y. Effects of axial inclined guide vanes on a turbo air classifier. *Powder Technol.* **2015**, *280*, 1–9. [CrossRef]
18. Yu, Y.; Ren, W.; Liu, J. A new volute design method for the turbo air classifier. *Powder Technol.* **2019**, *348*, 65–69. [CrossRef]
19. Sun, Z.; Sun, G.; Xu, J. Effect of deflector on classification performance of horizontal turbo classifier. *China Powder Sci. Technol.* **2016**, *22*, 6–10.
20. Yu, Y.; Liu, K.; Zhang, K. Establishment of a prediction model for the cut size of turbo air classifiers. *Powder Technol.* **2014**, *254*, 274–280. [CrossRef]
21. Molerus, O.; Hoffmann, H. Darstellung von windsichtertrennkurven durch ein stochastisches Modell. *Chem. Ing. Tech.* **1969**, *41*, 340–344. [CrossRef]
22. Betz, M.; Nirschl, H.; Gleiss, M. Development of a New Solver to Model the Fish-Hook Effect in a Centrifugal Classifier. *Minerals* **2021**, *11*, 663. [CrossRef]